Available online at www.sciencedirect.com
ScienceDirect
Trans. Nonferrous Met. Soc. China 30(2020) 2381−2393
Transactions of Nonferrous Metals Society of China
www.tnmsc.cn

Effect of inter-cycle heat treatment in accumulative roll-bonding (ARB) process on planar isotropy of mechanical properties of AA1050 sheets

Mojtaba DEHGHAN[1], Fathallah QODS[1], Mahdi GERDOOEI[2], Hamidreza MOHAMMADIAN-SEMNANI[1]

1. Faculty of Materials and Metallurgical Engineering, Semnan University, Semnan 35131-19111, Iran;
2. Faculty of Mechanical and Mechatronics Engineering,
Shahrood University of Technology, Shahrood 36199-95161, Iran

Received 6 December 2019; accepted 30 July 2020

Abstract: The accumulative roll-bonding (ARB) process was applied on the strips of aluminum alloy 1050 in two processing conditions: cold ARB and warm ARB. The results of tensile tests and microhardness measurement show that the warm ARB process exhibits the lower tensile strength and microhardness, more homogeneous distribution of the microhardness, higher elongation, and especially superior planar isotropy of the tensile properties in comparison to the cold ARB, because of the intermediate heat treatment as well as the elevated temperature rolling in the warm ARB process. Furthermore, with increasing the cycles of both processes, the planar isotropy decreases progressively.
Key words: aluminum; accumulative roll-bonding (ARB); intermediate heat treatment; mechanical properties; planar isotropy; hardness distribution

1 Introduction

Over the past decades, scientists paid considerable attention to the materials with ultrafine grain (UFG) microstructure due to their specific characteristics [1,2]. The researchers exerted severe plastic deformation (SPD) techniques to produce bulk materials with ultrafine grain microstructure and excellent mechanical properties [3−5], by applying large plastic strains [6,7].

Accumulative roll-bonding (ARB) process that was introduced by SAITO [8] in 1998, is one of the most effective SPD techniques for the manufacture of high-strength bulk sheet materials [9]. In brief, in the ARB process, two sheets are surface-prepared, stacked, and roll-bonded with a 50% reduction in thickness. Then, the rolled specimen is halved for the next cycle of the process. These stages are carried out for multiple cycles to attain a particular cumulated strain [10−12]. In the ARB method, an ultra-high plastic strain is exerted to the strip without any variation in its geometry. Consequently, large deformation and ultrafine grain microstructure are feasible by the ARB process [13,14]. The evolution of microstructure and mechanical properties of the ARB processed specimens is affected by inter-cycle heat treatment. The preheating stage in the ARB process is an effective factor for the occurrence of recovery and recrystallization phenomena and subsequently improvement of specimen properties [15].

FARHADIPOUR et al [16] fabricated AA5083−1%Al_2O_3 composite with warm ARB process. They illustrated that intermediate heating between the cycles of ARB led to recrystallization and grain growth in the metal matrix. WANG et al [17] produced Cu/Al composites by the ARB process at various rolling temperatures. They demonstrated a reduction in dislocation density and also the occurrence of grain coarsening with the increasing temperature. ABBASI and SAJJADI [18] evaluated

Corresponding author: Fathallah QODS; Tel/Fax: +98-23-33654119; E-mail: qods@semnan.ac.ir
DOI: 10.1016/S1003-6326(20)65386-9

the microstructure and mechanical characteristics of Al/Mg composites manufactured with warm ARB process. They reported that at high deformation temperature, grain growth took place. Also, they pointed out that high shear stress was applied in the interface regions due to friction between the layers. The shear band zones are the main locations for grain nucleation in the recrystallization. BOGUCKA [15] displayed that different structures contained elongated grains and also locally equaxial subgrains (arising from recovery and recrystallization processes) appeared in the AA5251 lamellar sheet produced with warm ARB at rolling temperature of 300 °C.

LI et al [19] investigated the restoration phenomena during annealing of the ARB processed commercially-pure aluminum. They found that continuous recrystallization occurred in the surface regions of the sample, and a mix of continuous and discontinuous recrystallization took place in the middle regions. KWAN et al [20] analyzed the microstructural development upon heating of the ARB deformed AA1100 strip. They showed that the dislocation density decreased, the equiaxial grains were attained, and the grain growth occurred after annealing at 250 °C. Besides, the aspect ratio of grains was reduced by increasing the annealing temperature. These results are in good accordance with the investigation performed by KAMIKAWA et al [21] on the high purity aluminum that was annealed after the ARB process. They demonstrated an increase of the grain size and a decrease of the aspect ratio of grains by increasing the time and temperature of annealing. KAMIKAWA et al [22] illustrated that heating of the ARB processed sample at 200 °C for a short time caused the recrystallization and grain growth in the structure.

In the studies on the ARB process, which investigated the influence of the heat treatment on the microstructure and mechanical properties of the specimens, lack of research to investigate the effect of the inter-cycle heating on the planar isotropy of the mechanical properties of samples is evident. For this reason, this study aims to examine the planar isotropy of tensile properties in the rolling plane of cold and warm ARB deformed samples. The further purpose of this research is to evaluate the homogeneity of microhardness distribution in the cold and warm ARB products.

2 Experimental

In this study, strips of the AA1050 alloy were used. The chemical composition of this alloy is presented in Table 1. Strips with thickness of 5 mm were firstly rolled to a thickness of 1 mm. Afterward, the specimens were annealed at 345 °C for 1 h to reach a recrystallized and equiaxed structure.

Table 1 Chemical composition of applied strip material AA1050 (wt.%)

Al	Si	Fe	Mn	Cr	Ni
99.54	0.172	0.157	0.010	0.0066	0.0019
Sn	Ti	Pb	Sr	V	Zr
0.0093	0.0044	0.0447	0.0002	0.0164	0.0371

In the ARB process, to attain a strong metallurgical bond, it is required to remove any pollutant that maybe exists on the surfaces of specimens. The best technique to reach high strength bonding between the samples is surfaces degreasing and then scratch brushing [23,24]. Hence, the surfaces of square specimens with 100 mm × 100 mm × 1 mm dimensions were cleansed in acetone and scratch brushed. Afterward, two of the cleaned samples were stacked together and fastened by copper wire to prepare them for the roll-bonding step. In subsequent step, the process was performed in two different modes. On one hand, the roll-bonding stage was carried out at ambient temperature (cold ARB). On the other hand, the specimens were preheated at 200 °C for 5 min before the rolling stage of ARB cycles and immediately roll-bonded (warm ARB). The strips were roll-bonded with a 50% reduction per cycle, with a laboratory rolling mill. The roll diameter was 110 mm, and the nominal strain rate was 12.4 s^{-1}. The deformed specimen was halved for the performing next cycle. To continue the process, the procedures, as mentioned above, were carried out up to 10 cycles. Figure 1 illustrates the ARB procedure schematically.

The microstructures of cold and warm ARB processed samples were investigated with a PHILIPS-XL scanning electron microscope (SEM). For the microstructural characterization, the rolling direction−normal direction(RD−ND) section of the

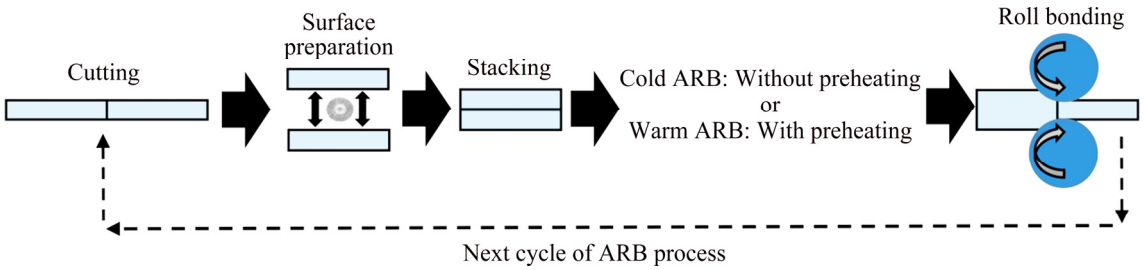

Fig. 1 Schematic illustration displaying principles of cold and warm ARB

specimens were polished and etched in a solution of 32 mL of diluted chromic acid (3 g chromic acid per 10 mL of H_2O), 40 mL Poulton's reagent (24 mL HCl + 12 mL HNO_3 + 2 mL H_2O + 2 mL HF), and 20 mL HNO_3.

To study the planar isotropy of tensile properties in rolling section of the deformed samples, the uniaxial tensile tests were carried out in several directions of specimens (rolling direction (RD), transverse direction (TD), and diagonal direction (DD)). The tensile test samples were prepared in a dog-bone-shape with a gauge length of 25 mm and a width of 6 mm (consistent with the subsize scale of the ASTM B 557M standard). Tensile tests were carried out at ambient temperature with a KSLAB03 tensile test machine. The tests were performed at a crosshead speed of 1.28 mm/min, which corresponded to a strain rate of 8.3×10^{-4} s^{-1}.

To evaluate the hardness distribution on the RD−ND section of the specimens, Vickers microhardness tests were carried out using a BUEHLER MMT−7 microhardness tester, with the spacing of 100 μm along the normal direction of the samples. The results of hardness tests were utilized for the computation of the mean microhardness and also the investigation of the microhardness distribution in the produced specimens.

3 Results and discussion

3.1 Microstructure

Figures 2 and 3 show SEM microstructures achieved from the RD−ND section of the strips deformed by cold and warm ARB methods, respectively. The annealed specimen, as the raw material, includes an equiaxed structure, with the mean grain size of 34 μm (Figs. 2(a) and 3(a)). After the initial cycle, the mean grain size in rolling and normal directions (d_{RD} and d_{ND}) decreases to 22.46 and 12.77 μm in cold ARB process, respectively (Fig. 2(b)), and 22.55 and 12.93 μm in warm ARB process (Fig. 3(b)). The grain size of the deformed samples is reduced continually, and the grains are elongated along the rolling direction with strain increment. Thus, the fraction of the ultrafine grain districts is enhanced by increasing the cycles. After 10 cycles, the d_{RD} and d_{ND} of the cold ARB products are around 1.91 μm and 420 nm, respectively (Fig. 2(e)), while in the warm ARB deformed strips these parameters are almost 2.05 μm and 590 nm, respectively (Fig. 3(e)). The d_{RD} and d_{ND} of the cold and warm ARB produced samples were measured with the linear interception method in the different sections of each micrograph, and the mean of the results of each micrograph is presented in Table 2.

In accordance with Table 2, by increasing cold and warm ARB cycles, the grains are elongated along the rolling direction, and the aspect ratio of grains (d_{RD}/d_{ND}) increases continuously, which is in good agreement with the research by SCHARNWEBER et al [25]. In the warm ARB deformed specimens, the aspect ratio of grains is lower; thus, the grains are more equiaxed in contrast to those in the cold ARB deformed samples. Besides, the grain size of the cold ARB deformed specimens is smaller in comparison with that of the warm ARB products. In the warm ARB process, due to the intermediate heat treatment as well as elevated temperature rolling, the grain size of the processed specimens is larger and also the grains are less elongated in comparison with the cold ARB process.

3.2 Tensile properties

The uniaxial tensile tests were carried out in the rolling, the transverse, and the diagonal

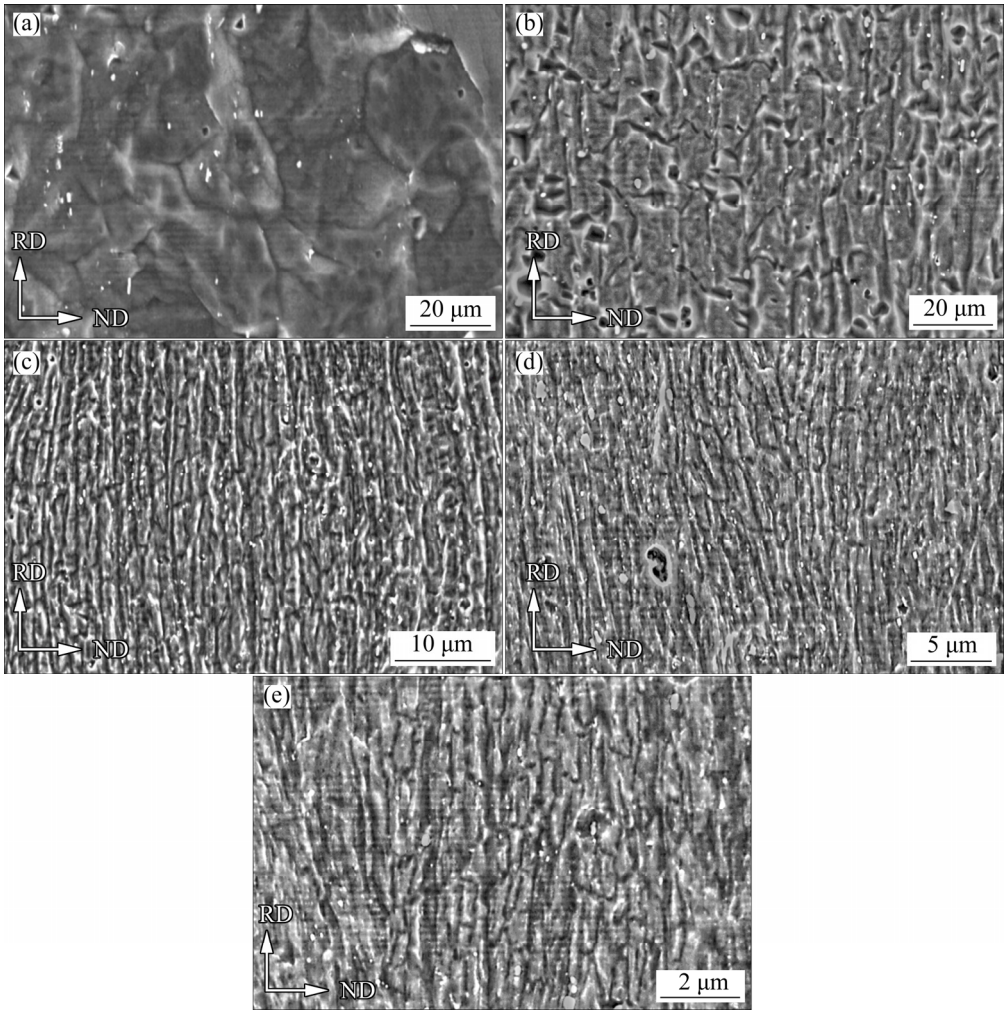

Fig. 2 SEM microstructures in RD−ND section of annealed sample (a) and strips after 1 (b), 4 (c), 7 (d) and 10 (e) cycles of cold ARB

directions of cold and warm ARB deformed strips after various cycles. The variations of the ultimate tensile strength (UTS), yield strength (YS), fracture elongation (fracture El.), and uniform elongation (uniform El.) with increasing the cycles of both processes are illustrated in Fig. 4. As seen, with the progression of the process, the tensile strength value increases continually. In the rolling direction, the tensile strength is enhanced remarkably from 69.25 to 128.5 and 121.25 MPa after the first cycle of cold and warm ARB processes, respectively, interestingly registering 86% and 75% enhancement in the strength. The same behavior is observed in the transverse and diagonal directions; after a cycle, the tensile strength increases by 98% and 71% in cold ARB specimens, and also by 85% and 65% in warm ARB specimens, respectively. Afterward, tensile strength increases continually until the tenth cycle in which the tensile strengths in the rolling direction get up to 201.7 and 185.05 MPa for the cold and warm ARB specimens, respectively. The data confirm 191% and 167% enhancement of the tensile strength in the cold and warm ARB products, respectively, in comparison to the initially annealed specimen. Ten cycles of cold and warm ARB could increase the tensile strength in the transverse direction by 221% and 193% compared to the un-deformed strip. The increase of the tensile strength in the diagonal direction is 162% and 143% for cold and warm ARB produced specimens after 10 cycles, respectively. As can be seen in Fig. 4, by the progress of the process, the rate of strength improvement is reduced, i.e., a type of saturation in the tensile strength happens. A similar trend is seen for the yield strength variations.

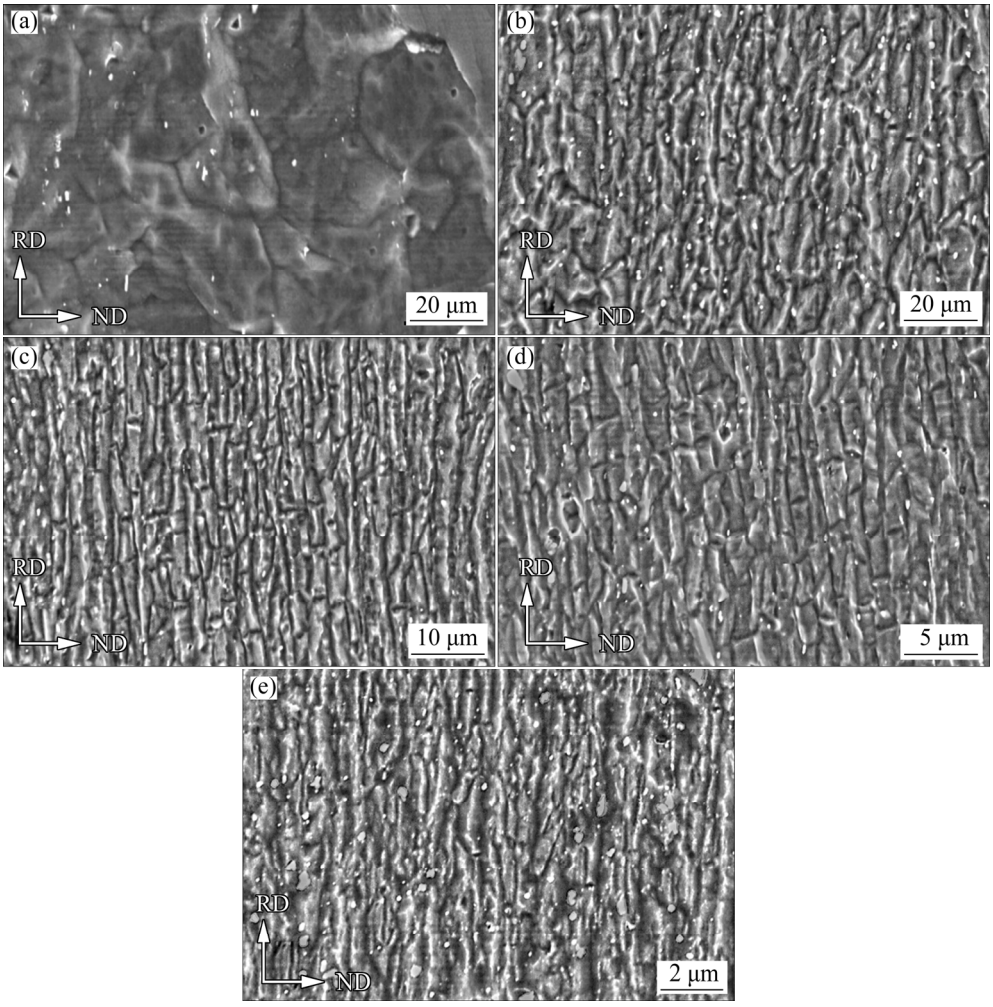

Fig. 3 SEM microstructures in RD−ND section of annealed sample (a) and strips after 1 (b), 4 (c), 7 (d) and 10 (e) cycles of warm ARB

Table 2 Mean grain size in rolling (d_{RD}) and normal (d_{ND}) directions and aspect ratio of grains (d_{RD}/d_{ND}) of cold and warm ARB produced strips

Sample	Cold ARB process			Warm ARB process		
	d_{RD}/μm	d_{ND}/μm	d_{RD}/d_{ND}	d_{RD}/μm	d_{ND}/μm	d_{RD}/d_{ND}
Annealed	34.4	33.7	1.02	34.4	33.7	1.02
1 cycle	22.46	12.77	1.76	22.55	12.93	1.74
4 cycles	6.48	1.89	3.43	7.11	2.36	3.01
7 cycles	4.1	0.96	4.27	4.32	1.31	3.30
10 cycles	1.91	0.42	4.55	2.05	0.59	3.47

It is obvious from Fig. 4 that the enhancing rate of strength by the progression of the warm ARB is lower compared to the cold ARB process. In the initial cycles of the cold and warm ARB processes, the plastic deformation causes an enhancement of the dislocation density and work hardening. In subsequent cycles of the warm ARB process, the dislocation density is approximately stable, due to the simultaneous occurrence of work hardening and work softening phenomena. In the softening phenomenon, the static and dynamic recoveries happen during inter-cycle heating and warm roll-bonding stages of the warm ARB process. As a result, the generation and annihilation of the dislocations are nearly balanced [18]. It should be mentioned that in higher cycles of the ARB process, the formation of ultrafine grains plays a remarkable role in the increase of the strength [24,26]. Thus,

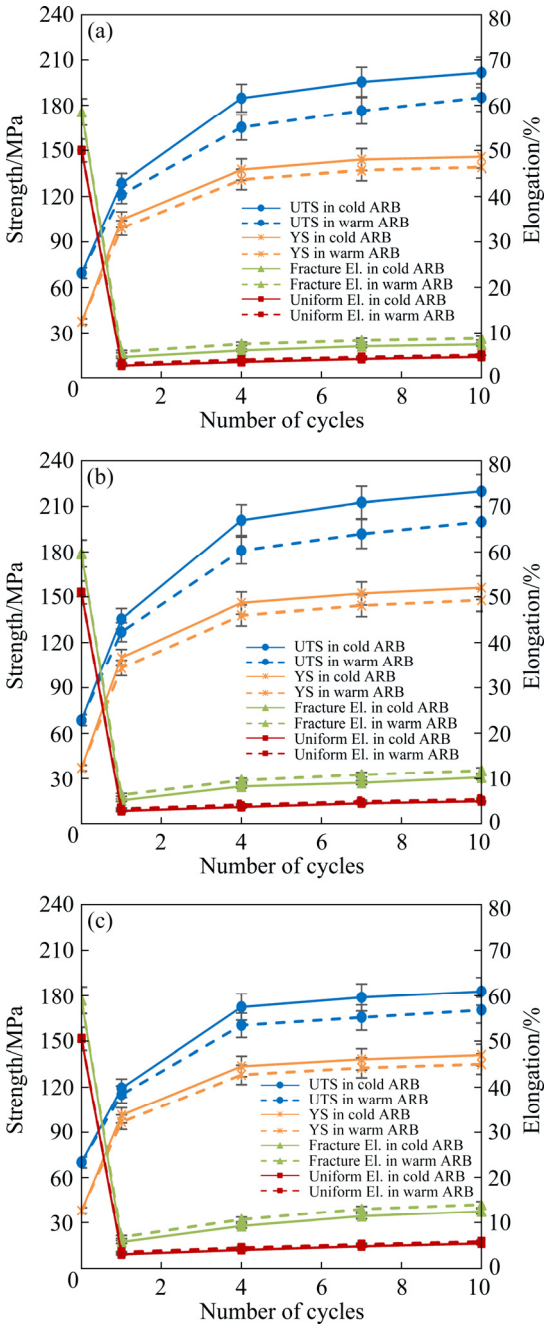

Fig. 4 Comparison of UTS, YS, fracture El. and uniform El. between cold and warm ARB processed samples in rolling (a), transverse (b), and diagonal (c) directions

the strength of warm ARB products is lower in comparison with that of the cold ARB ones, because of the larger grain size (according to the Hall−Petch equation) and lower dislocation density, which is obtained in the warm ARB process due to the intermediate heat treatment as well as the elevated temperature rolling in this process.

The variation of fracture elongation and uniform elongation of the cold and warm ARB processed samples are shown in Fig. 4. As illustrated, the elongation of the first cycle deformed strips decreases noticeably. In the rolling direction, the fracture elongation drastically drops from 58.5% for the un-deformed specimen to 4.6% and 5.8% for the one cycle cold and warm ARB processed samples, respectively, indicating 92% and 90% decrement. The same trend is seen in the transverse and diagonal directions; after a cycle, the elongation is reduced by 91% and 90% in cold ARB, and also by 89% and 88% in warm ARB, respectively. This considerable diminution is chiefly due to the extremely strain hardening caused by dislocations accumulation after the first cycle. Also, the de-bonding in the feeble interfaces of layers affects the decrease of ductility of the ARB products, significantly [27]. On the other hand, with the progression of the processes, the elongation improves slowly, which is more evident in the warm ARB method. The fracture elongation is enhanced gradually until the tenth cycle in which the fracture elongation in the rolling direction attains 7.4% and 8.75% for the cold and warm ARB products, respectively. Similar behavior is observed in the transverse and diagonal directions so that after ten cycles of processes, the fracture elongation reaches 10.3% and 12.4% in cold ARB, and also 11.8% and 13.9% in warm ARB, respectively. The uniform elongation approximately varies as same as fracture elongation.

The formability of the ARB processed strips increases with the improvement of the bonding quality between the layers [18,28]. The unbonded districts between the layers of the ARB processed samples contain significant amounts of discontinuities and porosities. These defects lead to development of the stress concentration as well as triaxial stresses in the specimen, as a result reducing the elongation. With the progress of the ARB process, the bonding quality is improved and thus the elongation of the strip is enhanced slowly. Also, the structural refinement and development of ultrafine grains by increasing the ARB cycles cause gradual improvement of the elongation of the processed samples [29,30]. The bimodal distribution of ultrafine grains microstructure in higher ARB cycles leads to the increase of the elongation of the specimens [31].

Figures 5 and 6 show the optical micrographs of the RD−ND plane of the strip processed by one, four, seven, and ten cycles of cold and warm ARB,

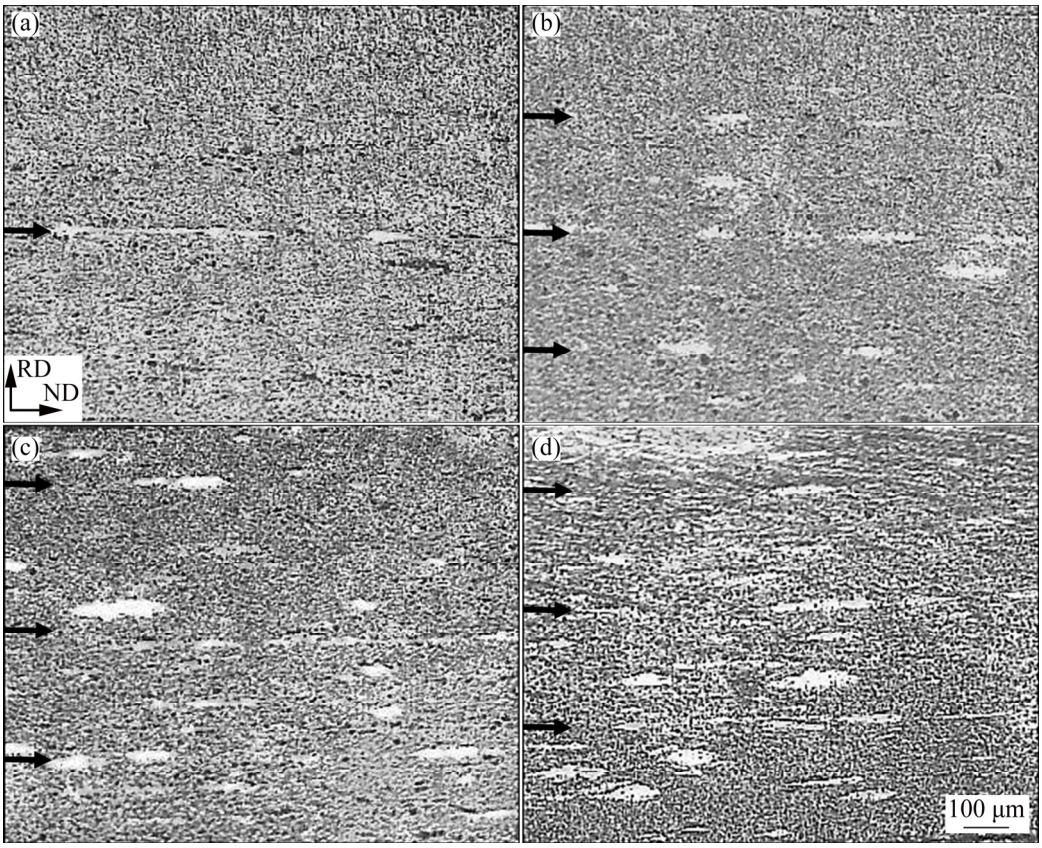

Fig. 5 Optical micrographs in RD−ND plane of samples after 1 (a), 4 (b), 7 (c) and 10 (d) cycles of cold ARB

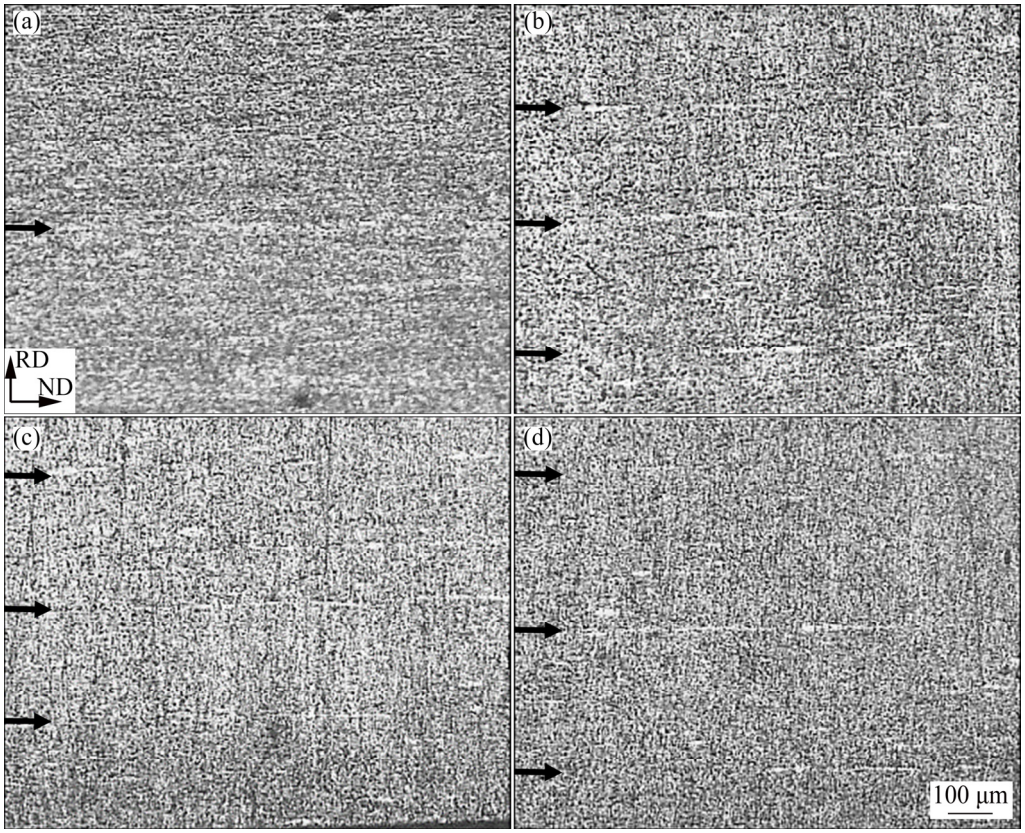

Fig. 6 Optical micrographs in RD−ND plane of samples after 1 (a), 4 (b), 7 (c) and 10 (d) cycles of warm ARB

respectively. The number of interfaces (N_i) after n cycles of the ARB process is calculated by

$$N_i=2^n-1 \quad (1)$$

For example, after 10 process cycles, 1023 (2^{10}–1) interfaces are produced. In Figs. 5 and 6, the interfaces of the last two cycles of processes are indicated by the arrows. As can be seen, only a few parts of the last bonded interfaces are observed in the samples, particularly in the warm ARB products. It is clear that the separation between the layers in the warm ARB processed specimens is less than that in the cold ARB ones, indicating better bonding quality in the warm ARB products. Thus, as can be observed in Fig. 4, the elongation of the warm ARB samples is higher in comparison with that of the cold ARB processed strips.

3.3 Planar isotropy

To investigate the planar isotropy of tensile properties in several directions (rolling direction, transverse direction, and two angles of ±45° toward the rolling direction (diagonal directions)) of the specimens, the uniaxial tensile tests are performed in these three directions of the products. The comparisons of the tensile properties among rolling, transverse and diagonal directions of the cold and warm ARB processed strips are demonstrated in Figs. 7 and 8, respectively.

The cold and warm ARB produced samples show very little uniform elongation (lower than ~6%). Hence, to examine the planar isotropy of tensile properties, the variation of Lankford value in several directions (the planar R-value) is not applied in the current research. Therefore, a variable parameter named as heterogeneity index (V) is exerted for the examination of planar isotropy in the rolling plane of specimens. The heterogeneity index is explained as a percentage of standard deviation (D_S) to the average value ($\bar{x}$) of the intended property (x), as follows [32,33]:

$$V=\frac{D_S}{\bar{x}}\times 100\% \quad (2)$$

where

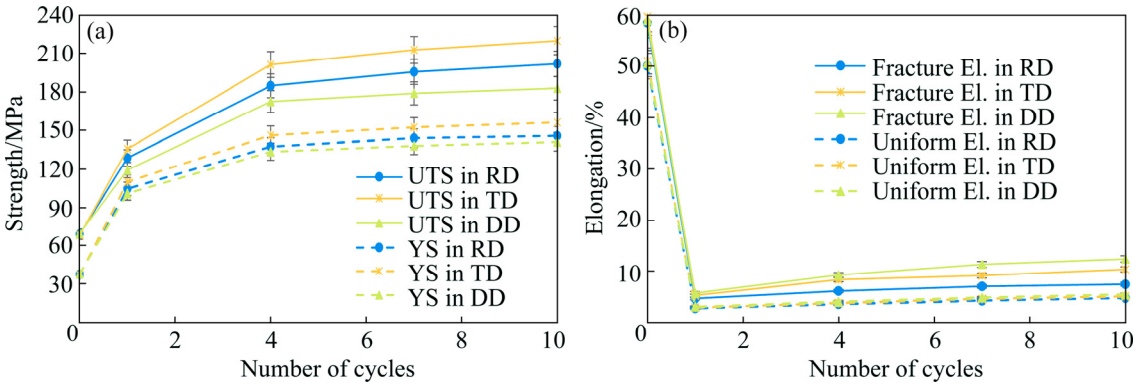

Fig. 7 Comparison of UTS, YS (a), fracture El., and uniform El. (b) among rolling (RD), transverse (TD) and diagonal (DD) directions of cold ARB processed samples

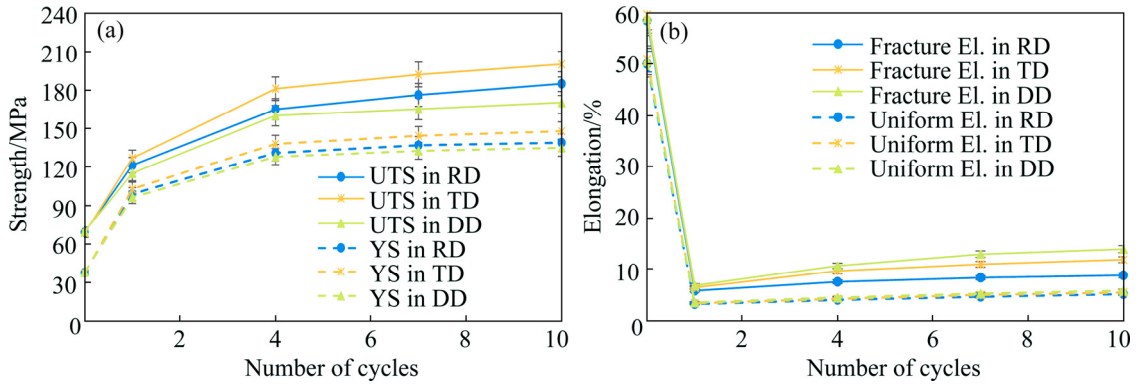

Fig. 8 Comparison of UTS, YS (a), fracture El., and uniform El. (b) among rolling (RD), transverse (TD) and diagonal (DD) directions of warm ARB processed samples

$$\overline{x}=\frac{x_{RD}+x_{TD}+2x_{DD}}{4} \quad (3)$$

and

$$D_S=\sqrt{\frac{1}{4}\sum_{i=1}^{4}(x_i-\overline{x})^2} \quad (4)$$

Figure 9 displays the variation of the heterogeneity index for the tensile strength and elongation of the deformed specimens as a function of cold and warm ARB cycles. As seen, with the progression of the processes, the heterogeneity index is enhanced continuously, as same as the increase of the aspect ratio of grains. When the grains are elongated, the planar heterogeneity of mechanical properties is enhanced; as a result, the planar isotropy of sheets is reduced.

According to Fig. 9, by comparing the heterogeneity index of cold ARB processed samples with warm ARB products, the planar heterogeneity of properties in the rolling section of the cold ARB produced specimens is higher in comparison with that of the warm ARB deformed strips. The warm ARB microstructure includes more equiaxed grains

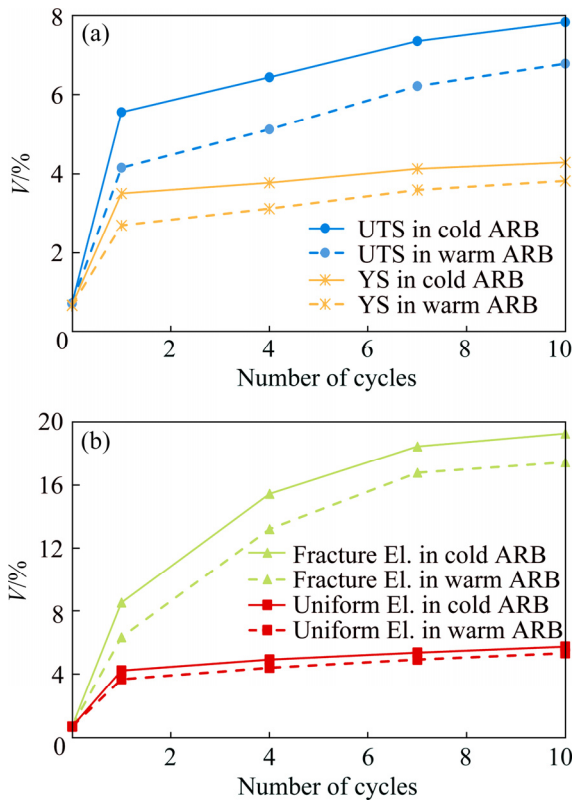

Fig. 9 Comparison of heterogeneity index value for UTS, YS (a), fracture El., and uniform El. (b) between cold and warm ARB processed samples

than the cold ARB microstructure, because of the inter-cycle heat treatment as well as the elevated temperature rolling in this process. Therefore, the planar isotropy of the warm ARB samples is higher than that of the cold ARB ones. Besides, this result is justifiable with texture analysis and also restoration phenomena in the literature.

It was shown that a through-thickness texture gradient is revealed in the ARB processed specimens. The rolling-type texture components are generated in the mid-thickness regions of the strips. In the subsurface regions, because of the significant friction between the specimen and the rolls and the occurrence of shear deformation in the surface region, the shear-type texture with the rotated cube component is developed [19,34,35]. In the cutting and stacking stages of the ARB process, half of the surface regions which contain shear texture components are moved to the central regions of the strip. The shear texture transfer into the strip interior can postpone the improvement of the rolling texture [34]. According to the full constraints Taylor model, the specimens with rolling texture components generally present higher planar anisotropy (Δr value), and on the contrary, the samples with rotated cube component typically exhibit lower planar anisotropy [35,36].

It must be noted that performing the ARB process with the preheating stage and subsequently warm roll-bonding, and as a result, promoting the friction condition can lead to the development of the shear texture with the rotated cube component. Thus, the planar anisotropy of the warm ARB products is lower compared to the cold ARB samples.

In the materials with the face-centered cubic (FCC) crystalline structure such as Al, the recrystallization and grain coarsening occur at lower temperatures [18]. Furthermore, the recovery and recrystallization phenomena take place more readily in the aluminum because of its high stacking fault energy (SFE). On the other hand, the SPD processes lead to decreasing the recrystallization temperature in the materials, due to the accumulated energy in them. It is noteworthy that the grain boundaries are suitable places for the grain nucleation [37,38]. Thus, in the specimens with ultrafine grain structure, the recrystallization happens more readily owing to more nucleation [39]. It must be noted that impurity absent in the pure Al can

lead to considerable recovery during the ARB process, which causes the formation of equiaxed grains beside lamellar grains in the microstructure [22]. The occurrence of recovery and recrystallization and nucleation of fine and equiaxed grains can decrease the influence of elongated grains and subsequently the anisotropy of the ARB product [7]. As mentioned above, the static recovery, recrystallization, and even grain growth phenomena during the inter-cycle heating stage and also the dynamic recovery and recrystallization during the warm rolling stage can occur in the pure Al strip that is processed by the warm ARB technique. Therefore, the anisotropy of the warm ARB processed strips is lower compared with that of the cold ARB products.

3.4 Microhardness distribution

To illustrate the hardness distribution, Vickers microhardness measurement was done throughout the thickness of the cold and warm ARB samples (Fig. 10). The microhardness is dispersed homogeneously in the studied section except in the near-surface regions. The higher microhardness of the subsurface districts is caused by significantly high shear strains in these regions, because of the friction between the rolls and specimens.

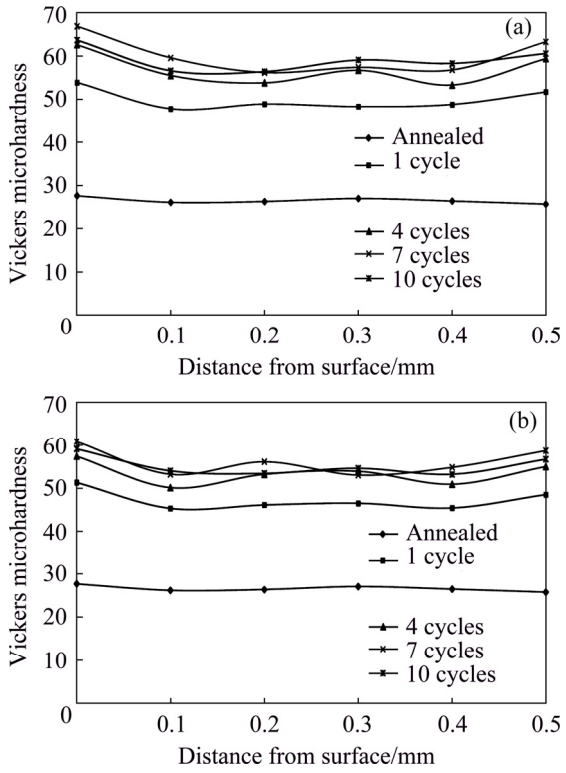

Fig. 10 Vickers microhardness distribution throughout thickness of cold (a) and warm (b) ARB processed products

The heterogeneity index of microhardness and the mean microhardness throughout the thickness (except near-surface outcomes) of the cold and warm ARB specimens are shown in Fig. 11. With increasing process cycles, the mean hardness is enhanced as same as strength enhancement. The increase of the microhardness by the progression of the processes is resulted from a large amount of exerted deformation as well as redundant shear strain in the interface districts of the deformed specimens. Figure 11 indicates that the mean microhardness is enhanced rapidly in the initial cycles and then increases gradually until the 7th cycle. Afterwards, the microhardness approximately remains stable until 10 cycles. This constancy is caused by the complicated distribution of the shear strain and saturation of the shear bands in the processed sample after several cycles [40,41]. Consistent with Fig. 11, in the high cycles of the processes, the heterogeneity index of microhardness is reduced slightly. This decrease can be attributed to the uniform distribution of the ultrafine grain microstructure as well as the saturation of the shear bands in the deformed strips in high roll-bonding cycles [41,42].

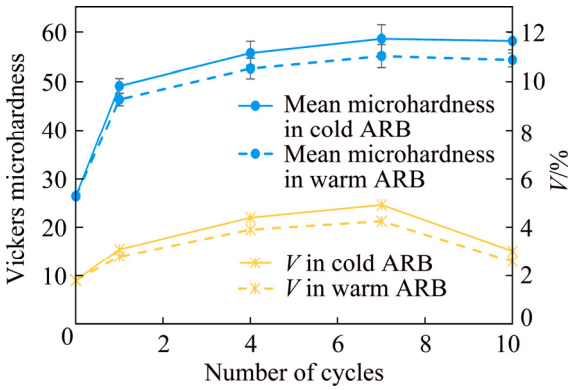

Fig. 11 Comparison of mean Vickers microhardness and heterogeneity index of microhardness between cold and warm ARB processed specimens after various cycles

According to Fig. 11, the mean hardness of the warm ARB processed samples is lower than that of the cold ARB processed ones. This discrepancy is explained by the occurrence of the softening mechanism and achieving a lower dislocation density in the warm ARB, because of the intermediate heating as well as the elevated

temperature rolling in this process. Besides, the heterogeneity index of microhardness in the warm ARB deformed strips is lower in comparison to that of the cold ARB deformed samples. This difference may be attributed to the fact that the recovery phenomenon in the warm ARB leads to the annihilation of dislocations that were cumulated in the microstructure during the process. Thus, the microhardness distribution in the warm ARB processed specimens is more uniform than that in the cold ARB products.

4 Conclusions

(1) Evaluation of the microstructure of cold and warm ARB products illustrates that by the progress of both processes, an ultrafine grain microstructure with elongated grains along the rolling direction is attained. The microstructure of cold ARB products contains more elongated and also finer grains than that of warm ARB ones.

(2) The strength of the warm ARB specimens is lower, and the elongation of them is higher compared to that of the cold ARB samples in the rolling, the transverse, and the diagonal directions of the products.

(3) With the progression of the cold and warm ARB, the planar isotropy of mechanical properties decreases continually.

(4) The planar heterogeneity of mechanical properties of the warm ARB deformed specimens is lower compared to that of the cold ARB deformed samples, because of the intermediate heat treatment as well as the elevated temperature rolling, which lead to the development of microstructure with more equiaxed grains and also rotated cube texture component and the occurrence of restoration phenomena in the warm ARB process. Thus, the warm ARB method presents better planar isotropy of the mechanical properties in comparison to the cold ARB technique.

(5) The mean microhardness of the warm ARB processed strips is lower compared to that of the cold ARB processed samples. Besides, the heterogeneity index of microhardness of the warm ARB products is lower in comparison with that of the cold ARB samples. This discrepancy is resulted from the more homogeneous distribution of the microhardness in the warm ARB specimens.

References

[1] BAGHERPOUR E, PARDIS N, REIHANIAN M, EBRAHIMI R. An overview on severe plastic deformation: Research status, techniques classification, microstructure evolution, and applications [J]. The International Journal of Advanced Manufacturing Technology, 2019, 100: 1647−1694.

[2] GASHTI S O, FATTAH-ALHOSSEINI A, MAZAHERI Y, KESHAVARZ M K. Effect of grain refinement on mechanical and electrochemical properties of ultra-fine grained AA1050 fabricated via ARB process [J]. Journal of Manufacturing Processes, 2016, 22: 269−277.

[3] LI X B, ZU G Y, WANG P. Microstructural development and its effects on mechanical properties of Al/Cu laminated composite [J]. Transactions of Nonferrous Metals Society of China, 2015, 25: 36−45.

[4] HOSSEINI A, RAHMATABADI D, HASHEMI R, AKBARI H. Experimental and numerical assessment of energy absorption capacity of thin-walled Al 5083 tube produced by PTCAP process [J]. Transactions of Nonferrous Metals Society of China, 2020, 30: 1238−1248.

[5] HONG X, GODFREY A W, LIU W. Anisotropic tensile behavior and related yield point phenomena in annealed ultrafine-grained pure aluminum [J]. Transactions of Nonferrous Metals Society of China, 2018, 28: 585−591.

[6] MOROVVATI M R, MOLLAEI-DARIANI B. The formability investigation of CNT-reinforced aluminum nano-composite sheets manufactured by accumulative roll bonding [J]. The International Journal of Advanced Manufacturing Technology, 2018, 95: 3523−3533.

[7] MOROVVATI M R, DARIANI B M. The effect of annealing on the formability of aluminum 1200 after accumulative roll bonding [J]. Journal of Manufacturing Processes, 2017, 30: 241−254.

[8] SAITO Y. Ultra-fine grained bulk aluminum produced by accumulative roll-bonding (ARB) process [J]. Scripta Materialia, 1998, 39: 1221−1227.

[9] SAITO Y, UTSUNOMIYA H, TSUJI N, SAKAI T. Novel ultra-high straining process for bulk materials — Development of the accumulative roll-bonding (ARB) process [J]. Acta Materialia, 1999, 47: 579−583.

[10] ZENG L F, GAO R, FANG Q F, WANG X P, XIE Z M, MIAO S, HAO T, ZHANG T. High strength and thermal stability of bulk Cu/Ta nanolamellar multilayers fabricated by cross accumulative roll bonding [J]. Acta Materialia, 2016, 110: 341−351.

[11] ZHAN M Y, LI Y Y, CHEN W P. Improving mechanical properties of Mg−Al−Zn alloy sheets through accumulative roll-bonding [J]. Transactions of Nonferrous Metals Society of China, 2008, 18: 309−314.

[12] CHEN X, HUANG G S, LIU S S, HAN T Z, JIANG B, TANG A T, ZHU Y T, PAN F S. Grain refinement and mechanical properties of pure aluminum processed by accumulative extrusion bonding [J]. Transactions of Nonferrous Metals Society of China, 2019, 29: 437−447.

[13] FATTAH-ALHOSSEINI A, NASERI M, ALEMI M H.

Corrosion behavior assessment of finely dispersed and highly uniform Al/B4C/SiC hybrid composite fabricated via accumulative roll bonding process [J]. Journal of Manufacturing Processes, 2016, 22: 120−126.

[14] DUAN J Q, QUADIR M Z, FERRY M. Engineering low intensity planar textures in commercial purity nickel sheets by cross roll bonding [J]. Materials Letters, 2017, 188: 138−141.

[15] BOGUCKA J. Influence of temperature of accumulative roll bonding on the microstructure and mechanical properties of AA5251 aluminum alloy [J]. Archives of Metallurgy and Materials, 2014, 59: 127−131.

[16] FARHADIPOUR P, SEDIGHI M, VINI M H. Influence of temperature of accumulative roll bonding on the mechanical properties of AA5083−1%Al_2O_3 composite [J]. Powder Metallurgy and Metal Ceramics, 2018, 56: 496−503.

[17] WANG L, DU Q L, LI C, CUI X H, ZHAO X, YU H L. Enhanced mechanical properties of lamellar Cu/Al composites processed via high-temperature accumulative roll bonding [J]. Transactions of Nonferrous Metals Society of China, 2019, 29: 1621−1630.

[18] ABBASI M, SAJJADI S A. Mechanical properties and interface evaluation of Al/AZ31 multilayer composites produced by ARB at different rolling temperatures [J]. Journal of Materials Engineering and Performance, 2018, 27: 3508−3520.

[19] LI S, YANG L, QIN N. Development of through-thickness texture gradient and persistence of shear-type textures during annealing of commercial purity aluminium sheet processed by accumulative roll-bonding [J]. Journal of Materials Science and Technology, 2018, 34: 821−831.

[20] KWAN C, WANG Z, KANG S B. Mechanical behavior and microstructural evolution upon annealing of the accumulative roll-bonding (ARB) processed Al alloy 1100 [J]. Materials Science and Engineering A, 2008, 480: 148−159.

[21] KAMIKAWA N, HUANG X, TSUJI N, HANSEN N. Strengthening mechanisms in nanostructured high-purity aluminium deformed to high strain and annealed [J]. Acta Materialia, 2009, 57: 4198−4208.

[22] KAMIKAWA N, TSUJI N, HUANG X, HANSEN N. Quantification of annealed microstructures in ARB processed aluminum [J]. Acta Materialia, 2006, 54: 3055−3066.

[23] JAFARIAN H, HABIBI-LIVAR J, RAZAVI S H. Microstructure evolution and mechanical properties in ultrafine grained Al/TiC composite fabricated by accumulative roll bonding [J]. Composites Part B: Engineering, 2015, 77: 84−92.

[24] MILNER J L, BUNGET C, ABU-FARHA F, KURFESS T, HAMMOND V H. Modeling tensile strength of materials processed by accumulative roll bonding [J]. Journal of Manufacturing Processes, 2013, 15: 219−226.

[25] SCHARNWEBER J, SKROTZKI W, OERTEL C G, BROKMEIER H G, HÖPPEL H W, TOPIC I, JASCHINSKI J. Texture, microstructure and mechanical properties of ultrafine grained aluminum produced by accumulative roll bonding [J]. Advanced Engineering Materials, 2010, 12: 989−994.

[26] TOROGHINEJAD M R, ASHRAFIZADEH F, JAMAATI R. On the use of accumulative roll bonding process to develop nanostructured aluminum alloy 5083 [J]. Materials Science and Engineering A, 2013, 561: 145−151.

[27] ALIZADEH M, PAYDAR M H. High-strength nanostructured Al/B_4C composite processed by cross-roll accumulative roll bonding [J]. Materials Science and Engineering A, 2012, 538: 14−19.

[28] RUPPERT M, HÖPPEL H W, GÖKEN M. Influence of cross-rolling on the mechanical properties of an accumulative roll bonded aluminum alloy AA6014 [J]. Materials Science and Engineering A, 2014, 597: 122−127.

[29] ALIZADEH M, SALAHINEJAD E. Processing of ultrafine-grained aluminum by cross accumulative roll-bonding [J]. Materials Science and Engineering A, 2014, 595: 131−134.

[30] ALIZADEH M, PAYDAR M H, JAZI F S. Structural evaluation and mechanical properties of nanostructured Al/B4C composite fabricated by ARB process [J]. Composites Part B: Engineering, 2013, 44: 339−343.

[31] NASERI M, REIHANIAN M, BORHANI E. Effect of strain path on microstructure, deformation texture and mechanical properties of nano/ultrafine grained AA1050 processed by accumulative roll bonding (ARB) [J]. Materials Science and Engineering A, 2016, 673: 288−298.

[32] ZENDEHDEL H, HASSANI A. Influence of twist extrusion process on microstructure and mechanical properties of 6063 aluminum alloy [J]. Materials and Design, 2012, 37: 13−18.

[33] ASHURI H, HASSANI A. Characterization of severely deformed new composites fabricated by powder metallurgy including a stage of mechanical alloying [J]. Journal of Alloys and Compounds, 2014, 617: 444−454.

[34] HIDALGO-MANRIQUE P, CEPEDA-JIMÉNEZ C M, OROZCO-CABALLERO A, RUANO O A, CARREÑO F. Evolution of the microstructure, texture and creep properties of the 7075 aluminium alloy during hot accumulative roll bonding [J]. Materials Science and Engineering A, 2014, 606: 434−442.

[35] SU L, LU C, GAZDER A A, SALEH A A, DENG G, TIEU K, LI H. Shear texture gradient in AA6061 aluminum alloy processed by accumulative roll bonding with high roll roughness [J]. Journal of Alloys and Compounds, 2014, 594: 12−22.

[36] SIDOR J, MIROUX A, PETROV R, KESTENS L. Microstructural and crystallographic aspects of conventional and asymmetric rolling processes [J]. Acta Materialia, 2008, 56: 2495−2507.

[37] MEHR V Y, TOROGHINEJAD M R, REZAEIAN A. Mechanical properties and microstructure evolutions of multilayered Al−Cu composites produced by accumulative roll bonding process and subsequent annealing [J]. Materials Science and Engineering A, 2014, 601: 40−47.

[38] QUADIR M Z, AL-BUHAMAD O, BASSMAN L, FERRY M. Development of a recovered/recrystallized multilayered microstructure in Al alloys by accumulative roll bonding [J]. Acta Materialia, 2007, 55: 5438−5448.

[39] BÖHM W, MERKLEIN M, LECHNER M. Innovative aluminium lightweight design by the combination of accumulative roll bonding and local intermediate heat treatment [J]. Materials Today: Proceedings, 2015, 2: 4992−4997.

[40] KOLAHI A, AKBARZADEH A, BARNETT M R. Electron back scattered diffraction (EBSD) characterization of warm rolled and accumulative roll bonding (ARB) processed ferrite [J]. Journal of Materials Processing and Technology, 2009, 209: 1436−1444.

[41] PIRGAZI H, AKBARZADEH A, PETROV R, KESTENS L. Microstructure evolution and mechanical properties of AA1100 aluminum sheet processed by accumulative roll bonding [J]. Materials Science and Engineering A, 2008, 497: 132−138.

[42] YAGHTIN A H, SALAHINEJAD E, KHOSRAVIFARD A. Processing of nanostructured metallic matrix composites by a modified accumulative roll bonding method with structural and mechanical considerations [J]. International Journal of Minerals, Metallurgy and Materials, 2012, 19: 951−956.

累积叠轧焊(ARB)工艺中循环间热处理对 AA1050 板材力学性能平面各向同性的影响

Mojtaba DEHGHAN[1], Fathallah QODS[1], Mahdi GERDOOEI[2], Hamidreza MOHAMMADIAN-SEMNANI[1]

1. Faculty of Materials and Metallurgical Engineering, Semnan University, Semnan 35131-19111, Iran;
2. Faculty of Mechanical and Mechatronics Engineering,
Shahrood University of Technology, Shahrood 36199-95161, Iran

摘　要：采用累积叠轧焊(ARB)工艺加工 1050 铝合金带材，分别在室温(冷 ARB)和 200 °C(热 ARB)两种条件下进行。拉伸测试和显微硬度测试结果表明，与冷 ARB 工艺相比，由于热 ARB 工艺中的中间热处理和高温轧制过程的作用，热 ARB 工艺加工的合金具有较低的抗拉强度和显微硬度，显微硬度分布更均匀，且具有较高的伸长率，特别是更优异的拉伸性能平面各向同性。此外，随着两种加工过程循环次数的增加，合金的平面各向同性逐渐减小。

关键词：铝；累积叠轧焊(ARB)； 中间热处理；力学性能；平面各向同性；硬度分布

(Edited by Bing YANG)